Materials Characterization 100 (2015) 68–73

Contents lists available at ScienceDirect

Materials Characterization

journal homepage: www.elsevier.com/locate/matchar

Study on the evolution processes from TiC_x to TiB_2 induced by B in Al melt

Jinfeng Nie [a,b,*], Yonghao Zhao [a], Enzhao Wang [b], Xiangfa Liu [b]

[a] Nano Structural Materials Center, School of Materials Science and Engineering, Nanjing University of Science and Technology, Nanjing 210094, China
[b] Key Laboratory for Liquid–Solid Structural Evolution and Processing of Materials, Ministry of Education, Shandong University, Jinan 250061, China

ARTICLE INFO

Article history:
Received 17 October 2014
Received in revised form 12 December 2014
Accepted 13 December 2014
Available online 15 December 2014

Keywords:
Aluminum alloys
TiC_x
Crystal growth
Crystal structure
Diffusion

ABSTRACT

The structural evolution from TiC_x to TiB_2 induced by the B element in the aluminum melt has been investigated and the possible evolution mechanism has been revealed. Based on the FESEM observations, it is found that the evolution takes place in three steps, i.e. the delamination of TiC_x, in situ crystallization of TiB_2 on the TiC_x nanolamellas, the orientated attachment and Ostwald ripening during the TiB_2 growing process.

1. Introduction

TiB_2 and TiC_x are important ceramic materials and have received increasing attention because of their excellent physical and mechanical properties, such as high melting point, superior hardness, high modulus, low coefficient of thermal expansion as well as high chemical stability [1]. They are widely used as refractory materials for cutting tools and wear resistant component, especially as reinforcing phases in composites [2,3]. Furthermore, both of them can act as the effective nucleating substrates for -Al grain in aluminum alloys during the solidification process, due to their good lattice matching as well as their specific physical and chemical properties [4,5].

However, it was found that TiC_x was unstable in the aluminum alloy melts and reacted with other elements (Al, Si, B, etc.) during the holding time, which influenced its application in Al–Ti–C grain refiners and metal matrix composites [6,7]. Although Al–Ti–B master alloys containing TiB_2 are the preferred choice for grain refinement of wrought aluminum alloy in industry, the agglomeration of TiB_2 particles is a serious disadvantage for the grain refinement in some cases [8]. It can cause many problems in some cases, such as the porosity, streaking in aluminum foils and internal cracking in extrusion billets. Thus, it is really urgent to take effective ways to control the growth and agglomeration of TiB_2 particles in aluminum alloy melt.

Recently, it was found that the structural instability and evolution of TiC_x induced by B element in Al melt were effectively used to prepare a kind of titanium diboride core–shell structure particles, which displayed an effective grain refining efficiency [9,10]. Furthermore, the size and morphologies of the TiB_2 particles can be effectively controlled during the transformation. However, the transformation mechanism has not yet been fully understood. Herein, a study on the evolution processes from TiC_x to TiB_2 has been taken. We report for the first time the observation of the exfoliation of TiC_x crystals induced by B in Al melt, and the in situ crystallization mechanism of TiB_2 on TiC_x nanosheets has been raised based on the FESEM observations.

2. Experimental procedure

The materials used are 99.7 wt.% commercial pure aluminum, 99.85 wt.% graphite powder with size about 10 μm, 99.5 wt.% pure titanium and Al–3B alloy. Firstly, Al–Ti–C was prepared by the melt reaction method and weight ratio of Ti: C was fixed at 4:1 with the normal composition of Al–2.2Ti–0.55C. The graphite, Ti and pure Al powders were mixed and ball milled for 9 h, and then cold-pressed into pellets. Subsequently, the pellets were added into the Al melt at 1200 °C to prepare Al–Ti–C. Then, the Al–Ti–C was re-melted to above 1100 °C and 0.75 wt.% B in form of Al–3B was added into the melt to induce the transformation of TiC_x. Then the alloy was poured after holding for 5 s, 30 s, 60 s, and 2 min, respectively.

In order to obtain TiC_x and TiB_2, the bulk samples were dissolved in a 10 vol.% HCl-distilled water solution to remove Al matrix. The solutions with remaining particles were centrifuged by a centrifugal extractor. After that, the collected sedimented particles were rinsed with distilled water and ethanol for several times and then desiccated. The extracted particles were characterized by field emission scanning electron microscope (FESEM, SU-70, Japan and FEI Quanta 250, US) equipped with an

* Corresponding author at: Nano Structural Materials Center, School of Materials Science and Engineering, Nanjing University of Science and Technology, Nanjing 210094, China.
E-mail address: niejinfeng@njust.edu.cn (J. Nie).

http://dx.doi.org/10.1016/j.matchar.2014.12.017
1044-5803/

energy-dispersive X-ray spectroscopy (EDS) and high resolution transmission electron microscopy (HRTEM, FEI Tecnai 20, US).

3. Results and discussion

Fig. 1a shows the FESEM image of TiC_x particles extracted from the above Al–Ti–C system. It can be seen that most of the TiC_x particles display the typical truncated octahedron morphology enclosed by eight smooth {111} and six {100} facets due to the non-equilibrium growth condition in the Al melt [11]. However, after the addition of B element into the Al melt for a short time, the six {100} facets on the TiC_x truncated octahedron turn to be rather rough as shown by the arrows in Fig. 1b and seem to be selectively etched as shown by the magnified picture. Meanwhile, the B element directly caused the etching of the eight edges corresponding to {110} planes and cracks were formed as shown by the arrows in Fig. 1c–d. It is known that the surface energy (γ) of the {110} and {100} facets is much higher than that of {111} [12,13]. In general, the surface with higher surface energy always has higher absorption energy and is more unstable during the transformation process in the melt. After Al-B alloy added in the melt, B atoms are prone to be absorbed on the {110} and {100} planes preferentially and then dope into the inner lattice structure of TiC_x due to lots of C vacancies. Meanwhile, lots of Ti–C bonds were broken and then C and Ti atoms diffused outward into the melt resulting in the rough surface and cracked edges. Thus, the transformation of TiC_x introduced by the B in the Al melts started from the selective etching on {100} and {110} planes at the initial stage.

With the prolonged holding time, {100} facets of TiC_x octahedron became more rough and then holes were formed as shown by the arrows in the Fig. 2a–b, and the cracks formed on the {110} edges were also broader. Furthermore, visible delamination on {111} surfaces can be seen in Fig. 2b–c and then lamellas with thickness about 50–100 nm were formed, which could also be defined as two-dimensional nanocrystals [14]. It indicates that the nanolamellas are separated and will exfoliate from the {111} surface layer by layer as seen in Fig. 2c–d. The delamination phenomena are supposed to be induced by the doping of B into the lattice structure of TiC_x and is confirmed by the EDS analysis as shown in Fig. 2e–f, in which the peaks of B element appear. It is supposed that the Ti–C bonding has been broken and Ti–B bonding has formed instead. So, the formation of cracks is considered to be a result from the broken Ti–C bonding and the outward diffusion of C atoms.

Fig. 3 displays the morphologies of the particles in the Al–Ti–C–B system after adding B for 60 s and it can be seen that lots of regular hexagonal prisms with submicron size have formed on the original nanolamellas of TiC_x as shown in Fig. 3a–c. Figs. 3e–f show the TEM images of the hexagonal platelets and the corresponding selected-area electron diffraction (SAED), which confirm that the regular hexagonal prism is the formed TiB_2.

It is suggested that TiC_x and TiB_2 could establish coherency between their most close-packed lattice planes, which are (111) of TiC_x and (0001) of TiB_2 [15]. The arrangement of Ti atoms in both of them is almost the same, as shown in Fig. 4. The degree of disregistry between the substrate phase and the crystalline phase can be measured by the Turnbull–Vonnegut equation:

$$\delta = \frac{|a_c - a_s|}{a_c} \times 100\% \tag{1}$$

where a_s and a_c are the interatomic distances of the substrate plane and crystalline plane, respectively. The lattice mismatch of TiC_x (111) plane and TiB_2 (0001) plane is:

$$\delta = \frac{\left|a_{TiB_2} - a_{TiC}\right|}{a_{TiB_2}} \times 100\% = \frac{|3.028 - 3.060|}{3.028} \times 100\% = 1.057\%.$$

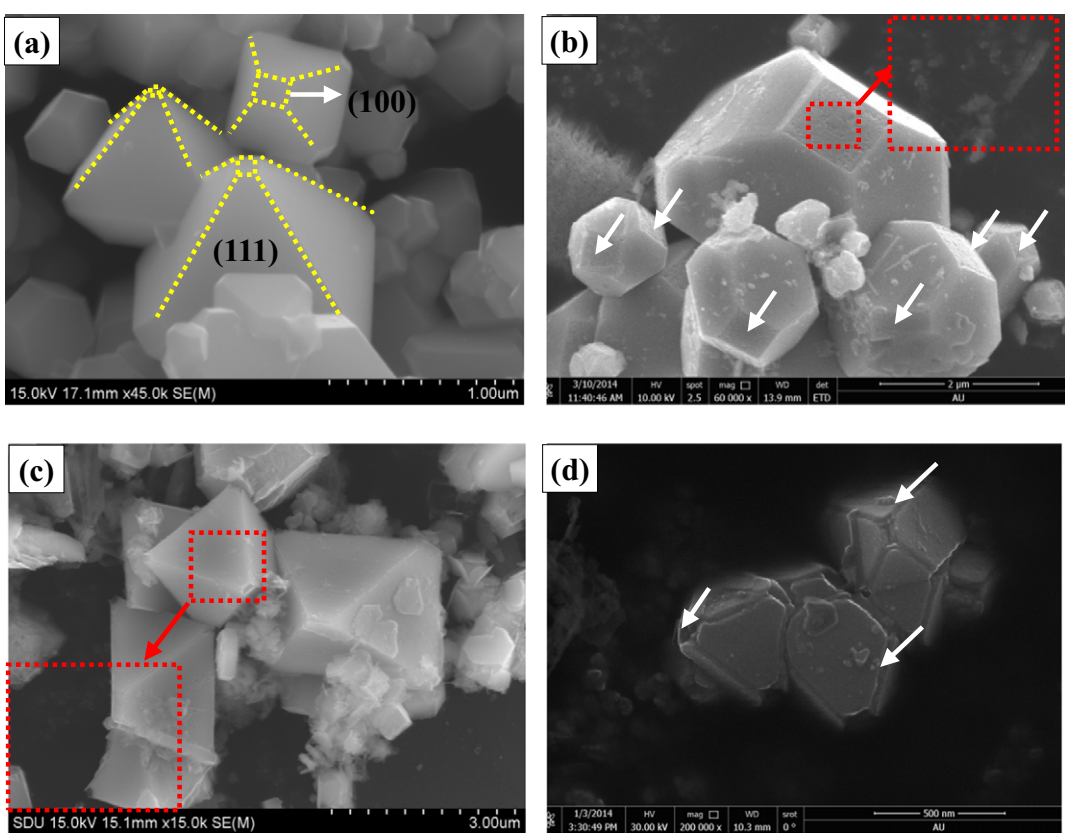

Fig. 1. Typical morphologies of TiC_x extracted from: (a) Al–Ti–C system; and (b–d) after B addition holding for 5 s.

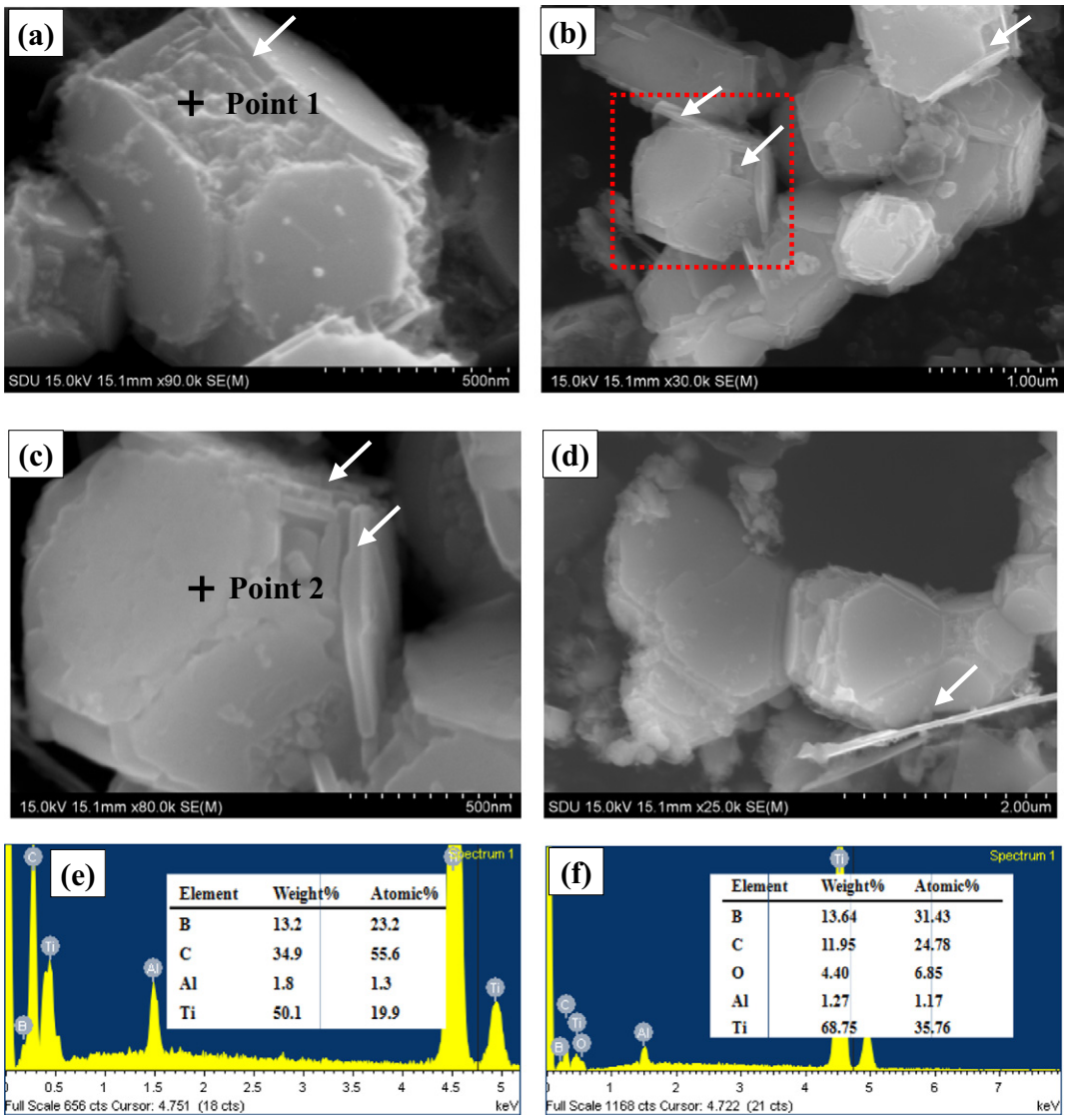

Fig. 2. Morphologies of TiC_x particles extracted from the Al–Ti–C–B system after B addition holding for 30 s (a–d) and the corresponding EDS analysis of Point 1 and Point 2 (e–f).

The result indicates that TiC_x (111) and TiB_2 (0001) are coherent interfaces. Thus, it is reasonable to believe that the surface of nanolamellas corresponding to {111} planes of TiC_x crystals can act as the nucleating substrates of TiB_2 crystals. It can be considered that the selective etching of {110} and {100} planes provides channels for atomic diffusion of B atoms and promotes the nucleation and growth of TiB_2. Furthermore, a piece of lamella may supply more than one nucleating site for TiB_2, and it can be seen that many small TiB_2 hexagonal prisms aggregate on the same surface as shown in Fig. 3a–b. The doping of more B atoms induce the broken of more Ti–C bonding and the gradual dissolution of TiC_x lamella, and then promotes the formation of Ti–B bonding and growth of TiB_2. Meanwhile, the TiB_2 hexagonal prisms nucleating on the same substrates share a common crystallographic orientation, and the regular oriented attachment is an important growth mechanism of these aggregates of TiB_2 to reduce the total interfacial energy [16]. Besides, the adjacent TiB_2 hexagonal prisms nucleating on different planes may connect with each other by certain planes as shown by Fig. 3d, which is referred as imperfect oriented attachment.

Fig. 5 shows the typical morphologies of particles extracted from the Al–Ti–C–B alloy after adding B for 2 min. Most of polyhedral TiC_x particles were transferred into hexagonal TiB_2, which indicated that the transformation process finished completely. Compared with Fig. 4, the width of most TiB_2 increased obviously and the edges became much smoother. It is considered that the growth of TiB_2 mainly occurs in this stage. Besides, some tiny particles can also be seen as shown in Fig. 5a. Therefore, it is supposed that the Ostwald ripening mechanism dominates the growth process of TiB_2, involving preferential dissolution of smaller TiB_2 particles and recrystallization and growth of larger TiB_2 particles [17,18]. Since the smaller particles have a lower thermodynamic stability and a higher surface to volume ratio [18], the ripening process leads to the slow disappearance of the small particles and the continuous growth of large particles to minimize the surface energy. The edges and corners of the left small TiB_2 hexagonal prisms become much smoother as shown in Fig. 5c, which also confirms the Ostwald ripening mechanism. It can be also noted that the larger TiB_2 particles are not regular hexagonal prisms, which is caused by the non-equilibrium state of the Al melt. According to the EDS result, trace amount of C is always detected in the TiB_2, which has been revealed in our previous study [9]. It is considered that the doping of trace C can introduce many lattice defects and distortion in the crystal structure of TiB_2 and may be another reason for the irregular hexagonal morphology.

It was found that the reaction between TiC and B to form TiB_2 was thermally favorable [19]. According to chemical thermal data provided by Liang and Che [20], the Gibbs' free energy for the following reaction at 1400 K is calculated about −412.6 kJ/mol, indicating the instability of

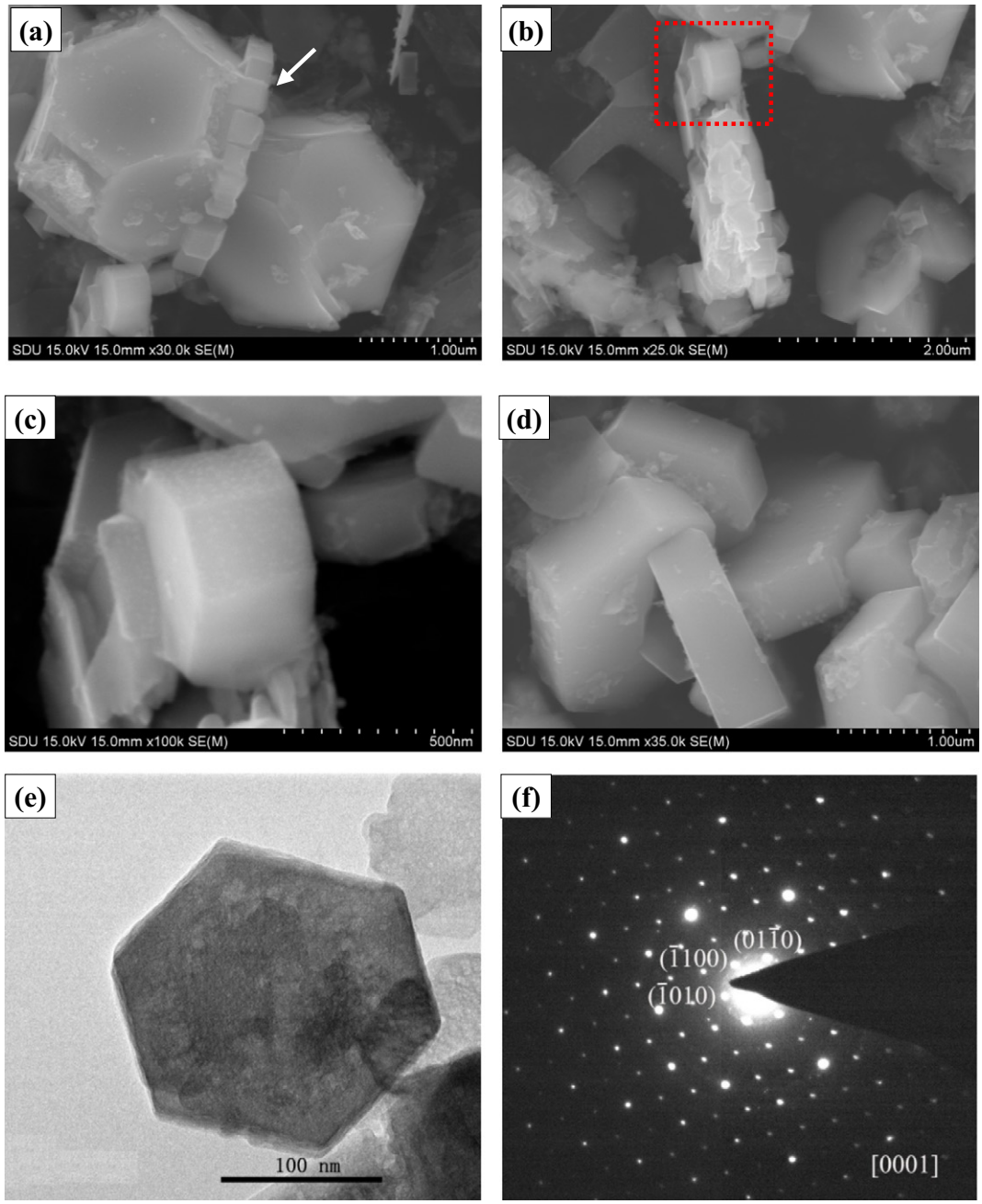

Fig. 3. Morphologies of extracted TiC_x and TiB_2 particles at the end of the transformation after holding for 60 s (a–d) and the corresponding TEM image and SAED pattern of hexagonal TiB_2 (e–f).

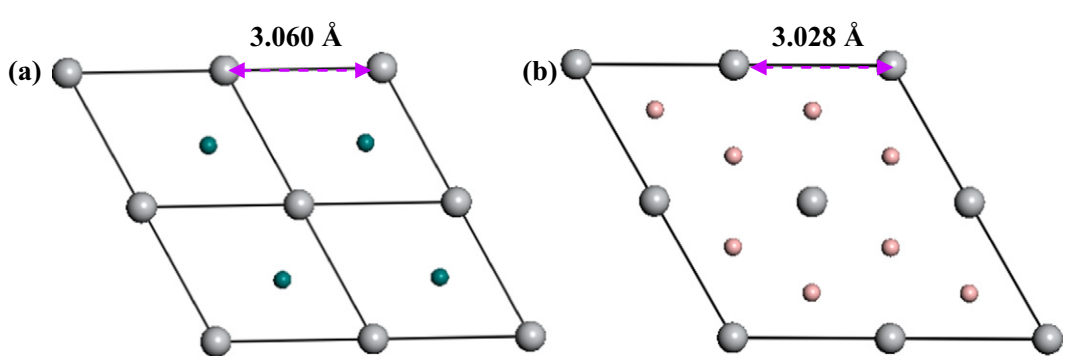

Fig. 4. The atom arrangement on: (a) TiC_x (111) and (b) TiB_2 (0001) planes. The gray balls denote Ti atoms, blue ones represent C atoms and the pink ones are B.

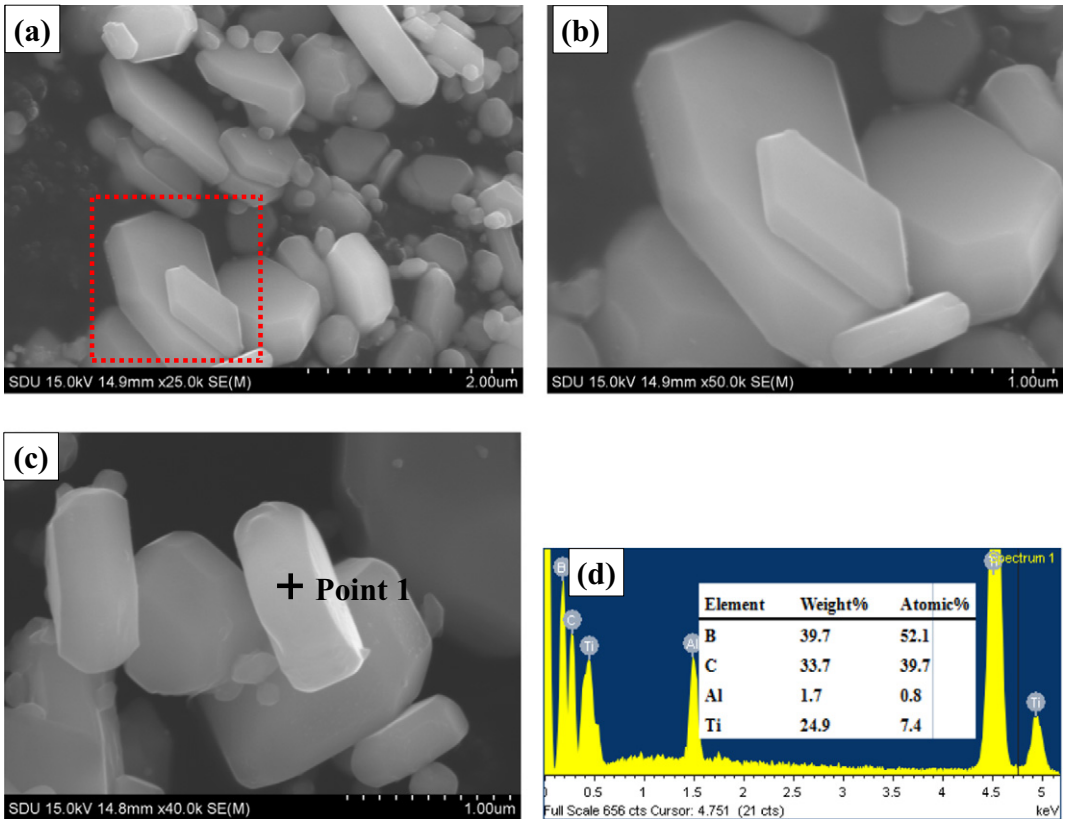

Fig. 5. FESEM images of TiB_2 particles extracted from Al–Ti–C–B system after adding B for 2 min: (a–c) typical morphologies of TiB_2; and (d) EDS analysis of Point 1.

TiC compared to TiB_2 in the Al melt. Besides, the C atoms diffused from the TiC_x combine with Al atoms surrounded to form the Al_4C_3 solid phase and then the reaction proceeds continually. Thus, the Al melt also promotes the reaction between TiC and B kinetically.

$$3TiC(s) + 6[B] + 4[Al] \rightarrow 3TiB_2(s) + Al_4C_3(s) \quad (2)$$

Base on the above analysis and observations, the evolution processes from TiC_x to TiB_2 can be divided into three steps and are tentatively summarized as follows. Firstly, the evolution starts from cracking of {110} edges and selective etching of {100} surfaces induced by the excess doping of B in the lattice crystal structure of TiC_x, the C vacancy defect in which also do favor for this process. Due to the strong covalent bond of Ti–B, the original of Ti–C bond is broken leading to the outward diffusion of C atoms. Because {111} is a kind of polar face with only Ti or C atoms on one layer, the broken Ti–C bond will lead to the weak bonding between {111} planes and to further delamination. Then, lots of nanolamellas with thickness smaller than 100 nm exfoliated from the {111} surfaces layer by layer.

We note that this is the first time that we reveal the delamination phenomena of TiC_x induced by the B element in the Al melt. Besides, Barsoum et al. reported a kind of new exciting 2D transition metal carbides Ti_2C, Ti_3C_2 produced by the exfoliation of Ti_2AlC, Ti_3AlC_2 and utilizing the selective etching of Al layers from the MAX phases in the HF treatment [14,21]. Inspired by their research results, it is supposed that 2D TiC_x could be produced in our system if the doping process of B was effectively controlled by the extremely low B concentration in order to impede the nucleation process of TiB_2, which will be studied in our future work.

Secondly, in the in situ crystallization of TiB_2 hexagonal prism from TiC_x, the exfoliated TiC_x nanosheet serves as the nucleating substrates of TiB_2 due to the crystal lattice match between TiC_x {111} faces and

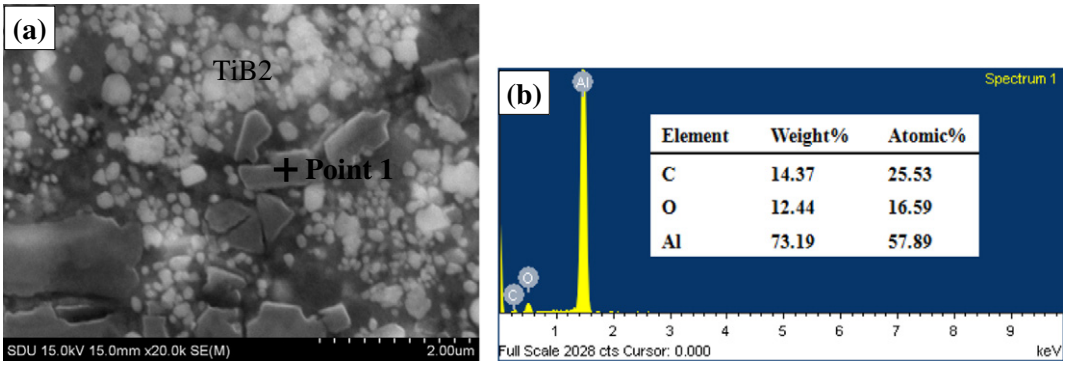

Fig. 6. Microstructures of the prepared Al–Ti–C–B alloys after adding B for 2 min (a) and the EDS analysis of Point 1 (b).

{0001} planes of TiB_2. The growth of TiB_2 nucleus is facilitated by the dissolution of TiC_x nanosheet and the deposition of B atoms. Moreover, a piece of lamella can supply many nucleating sites for TiB_2 hexagonal prisms, which share a common crystallographic orientation, thus regular oriented attachment becomes an important growth mechanism of these TiB_2 and then the hexagonal TiB_2 plates form. It is known that the growth of TiB_2 is limited by the exfoliation of TiC_x and the dissolution rate of the lamella, and vice versa. Thus, the growth rate of TiB_2 is relatively low compared with that formed by the direct reaction of B and Ti atoms in the Al melt at the similar melt reaction temperature [8,9].

Besides, Fig. 6a shows the microstructure of the prepared Al–Ti–C–B alloy after adding B for 2 min and it can be seen that the sub-micro white particles are TiB_2 distributed in the Al matrix. While the gray phase is Al_4C_3 which can be confirmed by the EDS result in Fig. 6b and indicates that the C atoms outward diffused from TiC_x combine with Al atoms surrounded. Lastly, the TiB_2 crystal continues to grow if the melt holding time is prolonged. Ostwald ripening mechanism dominates by the preferential dissolution of smaller TiB_2 particles and recrystallization and growth of larger TiB_2 particles.

4. Conclusions

In summary, the kinetic evolution processes from TiC_x to TiB_2 have been investigated. FESEM observations allow us to draw the conclusion that the evolution takes place in three steps, i.e. the gradual delamination of TiC_x, in situ crystallization of TiB_2 on the exfoliated TiC_x nanolamellas, the orientated attachment growth and Ostwald ripening during the TiB_2 growing process. The new findings here should let one better understand the similar evolution of transition metal carbides induced by the impurity element in the metal melt.

Acknowledgments

This research was financially supported by the National Natural Science Foundation of China (no. 51271101), China Postdoctoral Science Foundation (no. 2014M550292) and the Zijin Intelligent Program, Nanjing University of Science and Technology.

References

[1] S.K. Bhaumik, C. Divakar, A.K. Singh, G.S. Upadhyaya, Mater. Sci. Eng. A 279 (2000) 275–281.
[2] J.F. Li, F. Li, K. Hu, Y. Zhou, J. Eur. Ceram. Soc. 21 (2001) 2829–2833.
[3] G. Wen, S.B. Li, B.S. Zhang, Z.X. Guo, Acta Mater. 49 (2001) 1463–1470.
[4] G.S. Vinod Kumar, B.S. Murty, M. Chakraborty, J. Alloys Compd. 396 (2005) 143–150.
[5] H.M. Ding, X.F. Liu, L.N. Yu, G.Q. Zhao, Scr. Mater. 57 (2007) 575–578.
[6] A.R. Kennedy, D.P. Weston, M.I. Jones, Mater. Sci. Eng. A 316 (2001) 32–38.
[7] J.F. Nie, X.G. Ma, H.M. Ding, X.F. Liu, J. Alloys Compd. 486 (2009) 185–190.
[8] P.T. Li, Y.Y. Wu, X.F. Liu, Mater. Res. Bull. 48 (2013) 2044–2048.
[9] J.F. Nie, H.M. Ding, Y.Y. Wu, X.F. Liu, Scr. Mater. 68 (2013) 789–792.
[10] H.M. Ding, X.F. Liu, J.F. Nie, Mater. Charact. 63 (2012) 56–62.
[11] J.F. Nie, Y.Y. Wu, P.T. Li, X.F. Liu, CrystEngComm 14 (2012) 2213–2221.
[12] Y. Xia, Y. Xiong, B. Lim, S.E. Skrabalak, Angew. Chem. Int. Ed. 48 (2009) 60–103.
[13] L.H. Fang, L. Wang, J.H. Gong, H.S. Dai, D.Z. Miao, Trans. Nonferrous Metals Soc. China 20 (2010) 857–862.
[14] M. Naguib, M. Kurtoglu, V. Presser, J. Lu, J.J. Niu, M. Heon, L. Hultman, Y. Gogotsi, M.W. Barsoum, Adv. Mater. 23 (2011) 4248–4253.
[15] D. Vallauri, I.C. Atías Adrián, A. Chrysanthou, J. Eur. Ceram. Soc. 28 (2008) 1697–1713.
[16] R.L. Penn, J.F. Banfield, Science 281 (1998) 969–971.
[17] P.W. Voorhees, Annu. Rev. Mater. Res. 22 (1992) 197–215.
[18] P.W. Voorhees, J. Stat. Phys. 38 (1985) 231–252.
[19] O. Kubaschewski, C.B. Alcock, Thermochemical data, Metallurgical Thermochemistry, Pergamon, Oxford, 1979. 258.
[20] Y.J. Liang, Y.C. Che, Thermal Data on Inorganic Compounds, Northeast University of China, 1993. (in Chinese).
[21] M. Naguib, V.N. Mochalin, M.W. Barsoum, Y. Gogotsi, Adv. Mater. 26 (2014) 992–1005.